# Angular BAO Measurements with the DESI DR1 BGS Sample

Paula S. Ferreira<sup>1</sup> o a, Ulisses Ribeiro<sup>1</sup>, Pedro da Silveira Ferreira<sup>1,2</sup> o, Clécio R. Bom<sup>1</sup> o, and Armando Bernui<sup>3</sup> o

- <sup>1</sup> Centro Brasileiro de Pesquisas Físicas, CEP 22290-180, Rio de Janeiro, RJ, Brazil
- Observatório do Valongo, Universidade Federal do Rio de Janeiro, CEP 20080-090, Rio de Janeiro, RJ, Brazil
- Observatório Nacional, Rua General José Cristino, 77, São Cristóvão, 20921-400, Rio de Janeiro, RJ, Brazil

Received: date / Revised version: date

Abstract. We employ a model-independent approach in both the correlation function estimation and the angular BAO feature estimation by computing the angular two-point correlation function. First, we conducted a series of tests to the available DESI tracers to check their representativeness to angular clustering; the result was that, considering the completeness of the first data release across the footprint, we could only make use of the BGS sample for the effective redshifts 0.21 (BGS1) and 0.25 (BGS2). For a reliable analysis in such low redshift, we consider Lagrangian Perturbation Theory at first order on our mocks, which approximately reproduces the expected non-linearities, and generate the corresponding random catalogues. We use a purely statistical method to correct the projection effects and find that our results show reasonable agreement with the  $\theta_{\rm BAO}$  expected by the CPL parameters obtained by DESI DR1, being BGS1 11.78  $\pm$  1.12 degrees and BGS2 11.81  $\pm$  1.20 degrees. This means a tension at the 1.5 $\sigma$  (2.6 $\sigma$ ) level for BGS1 (BGS2) CPL parametrization, while a  $2\sigma$  (3.3 $\sigma$ ) discrepancy within the predicted by  $\Lambda$ CDM. We conclude that, with the current sample available, the use of an angular correlation function serving as the BAO probe, although prefers the CPL parametrization, does not provide conclusive results regarding the best cosmological model.

PACS. XX.XX.XX No PACS code given

# 1 Introduction

The Baryon Acoustic Oscillations (BAO) scale is imprinted on the large-scale structure of the universe from sound waves propagating in the primordial plasma. After recombination, these waves froze, leaving a characteristic scale, a standard ruler, of approximately 150 Mpc in the comoving frame. This physical scale provides a powerful geometric probe for measuring the expansion history of the universe and constraining the properties of dark energy.

Computing the two-point correlation function (2PCF) of the distribution of cosmic objects, the BAO feature appears as a peak [Eisenstein et al., 2005]. Alternatively, one can measure the Fourier-space equivalent of the 2PCF, that is, the power spectrum, where the BAO feature appears as a series of oscillations [Cole et al., 2005].

While the 3-dimensional (3D) analysis combines radial and transverse information to measure the Hubble parameter H(z) and the angular diameter distance  $D_A(z)$  simultaneously, the transverse BAO signal offers a complementary and robust approach. Complementing the BAO analysis in 3D matter distribution, one can also investigate the transverse BAO scale in thin redshift bins of matter distribution, where the BAO signature is expected as cir-

cular rings on the celestial sphere, with angular radius  $\theta_{\rm BAO}(z)$ .

As in the BAO-3D studies, the transverse BAO feature was also detected in the analysis of diverse cosmic tracers and at different epochs of universe evolution [Cole et al., 2005, Percival et al., 2010, Alam et al., 2017, Gil-Marín et al., 2020, Chan et al., 2022, DESI collaboration, 2025]. These studies not only confirm the BAO as a universal phenomenon, but, more interestingly, provide measurements of this standard ruler at several redshifts.

The concordance model of cosmology,  $\Lambda$ CDM, is being exhaustively tested with precise data recently released by the Dark Energy Spectroscopic Instrument (DESI) Collaboration [DESI Collaboration, 2025b,a,c]. In fact, the focus of this large astronomical survey is to obtain precise measurements of the BAO scale, by analyzing a series of cosmic tracers at different redshifts. Recently, statistical analyses of the DESI collaboration combined these BAO measurements with Planck CMB and supernovae type Ia data, concluding that the flat- $\Lambda$ CDM model is not the preferred model [DESI Collaboration, 2025c] with  $w_0 < -1$  and  $w_a \neq 0$ . Instead, the data favoured the  $\omega_0 \omega_a$ CDM model, with evolving dark energy, considering the CPL parametrisation [Chevallier and Polarski, 2001, Linder, 2003].

 $<sup>^{\</sup>rm a}~\mbox{\it e-mail:}$ psilf12@gmail.com

	BGS		LRG		ELG		QSO	
	$\overline{\text{SGC}}$	NGC	$\overline{\text{SGC}}$	NGC	$\overline{\text{SGC}}$	NGC	$\overline{\text{SGC}}$	NGC
Area (deg <sup>2</sup> )	3,035	6,829	3,497	5,934	3,436	5,845	3,473	5,875
Galaxies $(\times 10^3)$		1,048		1,476	611	1,821	430	793
Density $(deg^{-2})$	345	426	189	249	178	312	124	135

Table 1: Sky coverage by tracer type, showing area, galaxy counts, and number density. SGC and NGC refer to the Southern and Northern Galactic Caps respectively.

The goal of this work is to analyse the transverse BAO signal in low-redshift bins (low-z), using Sánchez et al. [2011] polynomial fit to obtain cosmological constraints and check whether DESI DR1 shows model-free BAO results for different fiducial cosmologies analysed by DESI Collaboration [2025c] projection effects.

#### 2 Data set

In this study, we use data from the first release (DR1)<sup>1</sup> by the DESI, a state-of-the-art spectroscopic instrument located at the 4-meter Mayall Telescope at Kitt Peak National Observatory in Arizona, USA [Levi et al., 2019]. DESI is now conducting a massive spectroscopic survey, mapping over 14,000 square degrees of the sky to measure the redshifts of tens of millions of galaxies and quasars. We assessed suitable tracers for angular clustering and determined, after several tests, that only the low-redshift galaxy samples are adequate. One of the biggest problems using DR1 is the inhomogeneity of completeness across the footprint, which is a major drawback considering an angular-based measurement.

#### 2.1 On the selection of the best samples

The inspection conducted for each tracer involved the assessment of three key parameters: first, the total count of objects; second, the fraction of sky covered; third, the density of galaxies per square degree per redshift bin for the Southern and Northern Galactic Caps. We applied a redshift bin width of  $\Delta z = 0.1$  specifically for Luminous Red Galaxies (LRGs), Emission Line Galaxies (ELGs), and Quasi-Stellar Objects (QSOs), see Table 1. However, this did not reveal any notable BAO features. Upon exploring more refined binning strategies, we discovered that the implementation of highly granular bin sizes proved impractical for any of the tracers, particularly within the context of a conventional analysis framework like the one introduced in this study. This observation, quite naturally, prompted us to address the challenge of identifying the most effective bin width.

Using the cosmological model  $\Lambda$ CDM, which is a good enough approximation for the selection tests, we conducted an estimation of the angular scale associated with the BAO

Tracer	$z_{ m eff}$	bin	number of objects	
BGS NGC3	0.27	$0.26 \le z < 0.28$	168,440	
BGS NGC4	0.31	$0.30 \le z < 0.32$	120,925	
BGS NGC5	0.33	$0.32 \le z < 0.34$	104,837	
BGS SGC1	0.25	$0.24 \le z < 0.26$	65,461	
BGS SGC2	0.27	$0.26 \le z < 0.28$	$60,\!372$	
BGS SGC3	0.29	$0.28 \le z < 0.30$	53,020	
QSO NGC	1.52	$1.00 \le z < 2.00$	458,790	
LRG NGC	0.82	$0.70 \le z < 0.95$	714,089	
BGS NGC1	0.21	$0.20 \le z < 0.22$	212,411	
BGS NGC2	0.25	$0.24 \le z < 0.26$	179,202	

Table 2: Bins with enough clustered galaxies that could contain the BAO feature. The samples we suited to this analysis are in the bottom of the table.

signal within a circular region, examining different bin widths to assess its impact. Subsequently, we identified the specific data bins that would enclose such regions, ensuring that each contained a minimum of 500 galaxies. With these bins selected, the subsequent phase involves applying tests on the angular two-point correlation function (2PCF) to investigate the structure within the data. From this analysis, the remaining candidate bins are written in the Table 2, where

$$z_{\text{eff}} = \frac{\sum_{i < j} \rho_i \rho_j (z_i + z_j)}{2 \sum_{i < j} \rho_i \rho_j}, \qquad (1)$$

with i and j being the indices of each galaxy and  $\rho$  the WEIGHT\_SYS [Ross et al., 2025].

#### 2.2 Bins choice

Based on the DESI limitation due to fiber collisions, any angular counting should be greater than 0.05 degrees [Pinon et al., 2025]. The best resulting samples based on the selection described above were the BGS NGC1 and NGC2. Our bins seem to agree with the analysis by Novell-Masot et al. [2025a] who dropped the ELG sample for 3D clustering due to systematics that are better managed by the DESI Collaboration. The only difference is that we dropped the QSO sample because the resulting bin would suffer considerably with projection effects.

Some important notes must be added regarding BGS, we chose not to cut the mask into a more uniform one for a clearer correlation function for two reasons: first,

https://data.desi.lbl.gov/public/dr1/survey/ catalogs/dr1/LSS/iron/LSScats/v1.5/

# $N_{grid} = 1024 \\ N_{side} = 1024 \\ N_{side} = 1024$ Tracer Kernel: $\Theta(z < 0.1)$ $\Omega_m$ :0.3153 $\Omega_{\Lambda}$ : 0.6847 $\omega$ : -1.0 $\alpha_s$ : 0.9649 $\sigma_8$ : 0.8111 Transfer funtion: eiseinteins\_hu Galaxy bias: $b(z) = \sqrt{1+z}$

Table 3: Colore parameters used for mock realizations.

it would not be an interesting analysis to compare with the DESI Collaboration; second, cutting a rectangular area could introduce a biased analysis with structures particular to that region, especially when using the BGS sample. Moreover, we do not use the lowest redshift range from BGS because we would require accurate mocks to closely reproduce local non-linearities and also to introduce a representative model to fit the angular clustering [Novell-Masot et al., 2025b].

#### 2.3 Mocks

Because the BGS sample is susceptible to local inhomogeneities, we must make an effort to construct mock realisations that take these inhomogeneities into account. DESI Collaboration has carefully studied the ideal mock realisations to their samples and, as previously done by SDSS, has chosen to use 100 realisations from EZmocks [Chuang et al., 2015] based on improvements to the Zeldovich approximation (ZA). The ZA defines a Lagrange-space regime that leads to quasi-nonlinear solution, which breaks beyond quasi-nonlinear due to caustics occurrence.

Here, we will use Colore [Ramírez-Pérez et al., 2022] to produce mocks using Lagrangian Perturbation Theory (LPT) whose description has intrinsically non-linear information [Bernardeau et al., 2002]. We chose to use first-order LPT (LPT1). In Ramírez-Pérez et al. [2022], Colore has tested its potential to generate stage-IV survey simulations that include the BGS sample.

The fiducial cosmology chosen to construct the mocks is based on Planck 18 results Planck Collab. [2020]; see Table 3 for 1,000 realisations for each tracer. We use a single random catalogue for the realisations, like the DESI Collaboration, these randoms have  $\sim 82$  times the number of the mock galaxies. Fig. 1 shows an example of a mock realisation for the BGS NGC samples. They have exactly the sky footprint of the real data.

The choice for  $\Lambda$ CDM fiducial cosmology is not in violation of the results obtained by the DESI Collaboration that favor the CPL model. The conditions for what is supposed to be a fair sample for an ensemble of universes were first postulated by Peebles [1973]. Our objective is to determine the size of the BAO peak. Therefore, a precise match between mock and observed data is unnecessary; we

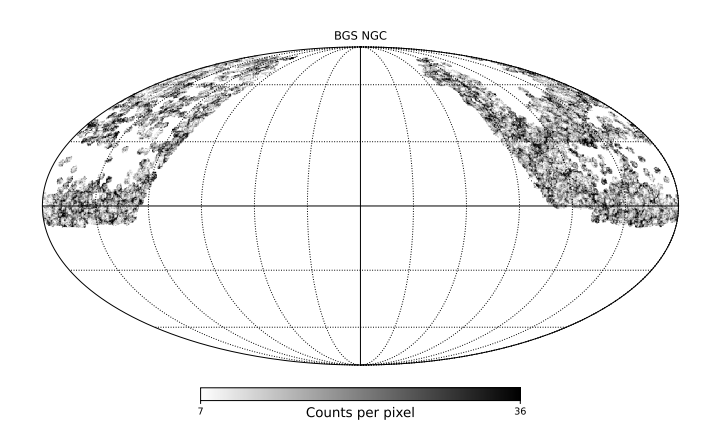


Fig. 1: BGS example mock. The darker regions indicate the most populated pixels.

only need to capture the same statistical distribution. It is essential to note that we are analysing the 2D correlation function, excluding the 3D component, and without relying on a fiducial cosmology for distance relation. Our primary concern is ensuring that the mocks fall within the correct mask and have sufficient number density.

The number of mocks followed the suggested rule of thumb by Hartlap et al. [2006], where the ratio

$$\frac{N_{mocks} - N_{data\;points} - 2}{N_{mocks} - 1}$$

should not be small ( $\ll 1$ ) in order to find good constraints. For a realistic pair counting, we estimated the mocks' weights using a Nearest-Neighbour interpolation with the observed data's right ascension, declination and redshift as the input variables to find the WEIGHT\_SYS.

# 2.4 Random catalogs

We construct random catalogs with a density 100 times larger than that of the data for the BGS (NGC) sample. The survey footprint is represented as the set of <code>HEALPix</code> pixel IDs at NSIDE =  $2^{29}$ . At this resolution, the full sky is a discrete grid of  $N_{\rm pix} \simeq 3.46 \times 10^{18}$  pixels, hence the BGS ( $f_{\rm sky} \simeq 0.16$ ) footprint corresponds to  $\simeq 5.6 \times 10^{17}$  admissible pixel IDs. For each random object, we sample uniformly from this grid of possible positions and assign the direction of the corresponding pixel center; this ID-based sampling avoids enumerating the full grid and is computationally very efficient. We then draw a redshift from the empirical N(z) of the matching sample (or tomographic bin), so that the randoms reproduce the observed radial selection.

By construction, these randoms are isotropic within the angular mask, as expected for a HEALPix grid map, and match the data's redshift distribution, while the  $100 \times$  larger size suppresses shot noise in pair counts. The extremely fine NSIDE makes any residual pixelization negligible. Nevertheless, our implementation can randomly perturb positions to remove any center-of-pixel imprint.

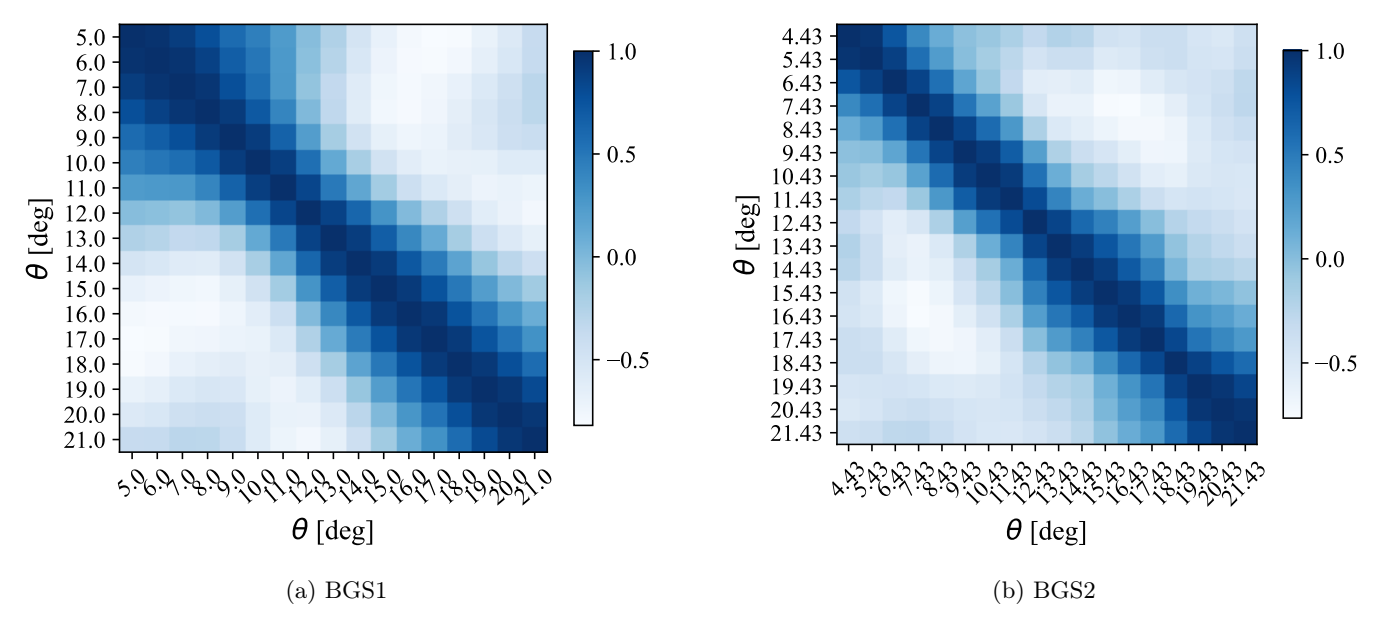


Fig. 2: Correlation matrix from the covariance of the 1,000 mock 2PCFs for BGS1 and BGS2.

At the grid resolution used, each pixel has a characteristic angular radius of  $\sim 2 \times 10^{-4}$  arcsec, and we verified that such a displacement has no measurable impact. The same procedure is in all correlation-function measurements.

# 3 Methodology

#### 3.1 Estimator

Utilizing the counts of pairs, the angular two-point correlation function for each redshift bin was calculated through the application of the Landy-Szalay estimator [Landy and Szalay, 1993]. For each angular function, normalization was carried out corresponding to the respective i-th tracer. The expression for the angular correlation function, denoted as  $\mathbf{w}_i$ , pertaining to the i-th bin, is represented by the equation provided below

$$\mathbf{w}_{i}(\theta) = \left(\frac{N_{i,rand}}{N_{i,data}}\right)^{2} \frac{DD_{i}(\theta)}{RR_{i}(\theta)} - 2\frac{N_{i,rand}}{N_{i,data}} \frac{DR_{i}(\theta)}{RR_{i}(\theta)} + 1 , (2)$$

where  $N_{i,rand}$  is the number of galaxies in the random catalog, and  $N_{i,data}$  in a tracer. The counting is based on WEIGHT\_SYS [Ross et al., 2025], we are not using Feldmann-Kaiser-Peacock's [Feldman et al., 1994] weight becase it is model-dependent and only affects the 3D clustering, our analysis is purely angular.

To substantiate the reliability of our methodology, we require the acquisition of survey catalogue realisations derived from simulated catalogues, commonly known as mocks. These mocks serve as an approximate representation of a survey, paying particular attention to its spatial coverage and redshift distribution. It is crucial to acknowledge that during the analysis of clustering statistics, one

major challenge posed by these mocks is the accurate representation of nonlinear effects, which become unavoidable at lower redshift values as highlighted by previous studies.

In our study, we employ mocks to calculate  $\mathbf{w}_k(\theta)$  for the k-th mock, enabling us to rigorously evaluate the proposed method. At this juncture, the covariance matrix  $C_{ml}$  becomes an integral component:

$$C_{ml} = \frac{n_{\text{eff}}^{-1}}{N-1} \sum_{k=1}^{N=1000} [\mathbf{w}_k(\theta_m) - \bar{\mathbf{w}}(\theta_m)] \times [\mathbf{w}_k(\theta_l) - \bar{\mathbf{w}}(\theta_l)],$$
(3)

where  $\bar{\mathbf{w}}$  is the average over the correlation function  $\mathbf{w}_k(\theta)$  of each mock. The covariance matrices can be found in Fig.2, all three sets are showing a strong diagonal structure with minimal off-diagonal signals.

# 3.2 Model

We used Sánchez et al. [2011] expression below for the angular two-point correlation function to fit our estimated function

$$w(\theta) = A + B\theta^{\gamma} + Ce^{-\frac{(\theta - \theta_{fit})^2}{2\sigma^2}}.$$
 (4)

The parameter A is associated with how the function behaves following the BAO peak. The parameters B and C serve to quantify the significance of their corresponding terms; notably, if there is an absence of a BAO peak, then C will be set to zero. The variable  $\gamma$  describes the power-law nature of the function's general form. The physically significant parameters include  $\theta_{fit}$  and  $\sigma$ ; specifically,  $\theta_{fit}$  determines the location of the BAO, whereas  $\sigma$  defines the BAO's width. This approach has been used in several analyses, first by Carvalho et al. [2016], tested first

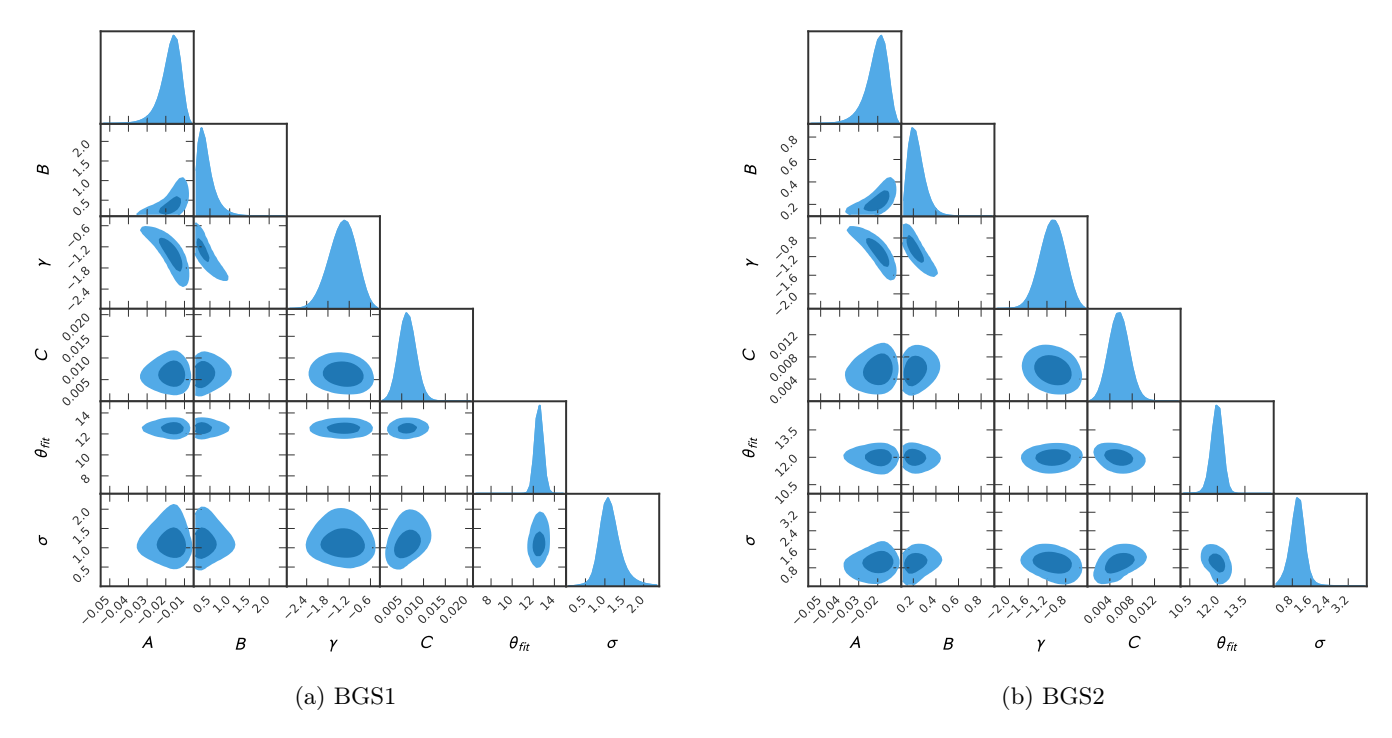


Fig. 3: BGS Best-fit to the model-free polynomial. Darker: 68% CL; lighter: 95.45% CL (MCMC posterior regions).

by Salazar-Albornoz et al. [2014] and later in low-z sample by Alcaniz et al. [2016]. The following papers were then a continuation of the methodology used: De Carvalho et al. [2018], Carvalho et al. [2020], De Carvalho et al. [2021, 2020], Menote and Marra [2022], Ferreira and Reis [2024], Ribeiro et al. [2025], additionally, Marra and Chirinos Isidro [2019] measured the BAO radial feature using the same polynomial function but applied to the redshift space.

We applied flat priors to the parameter C>0,  $10<\theta_{fit}<20$ ,  $0<\sigma<4$ , and B>0. The estimation of parameters was conducted employing the method of maximum likelihood estimation, using the Affine Invariant Markov Chain Monte Carlo (MCMC) Ensemble sampler as implemented in the emcee software, as detailed by Foreman-Mackey et al. [2013].

The sampling strategy employs a hybrid approach for generation. Approximately 80% of the proposed moves utilize a Differential Evolution Markov Chain Monte Carlo (DE-MCMC) algorithm Nelson et al. [2013], implemented in emcee as the DEMove. This method generates a candidate position for a given walker by taking a vector difference between two randomly selected companion walkers from the current ensemble, scaling it, and adding it to a third. The remaining 20% of moves are governed by the DESnooker algorithm Ter Braak and Vrugt [2008]. This move is designed to promote global exploration by proposing longer-range jumps. It operates by projecting a walker's position along a line defined by other points in the ensemble. The combination of these two moves leverages the efficiency of the DEMove for detailed sampling while using the DESnooker

Parameter	BGS1	BGS2
$\overline{}$	$0.006 \pm 0.002$	$0.0056 \pm 0.002$
$\theta_{fit}[\deg]$	$12.54 \pm 0.23$	$11.97 \pm 0.27$
$\sigma  [\mathrm{deg}]$	$1.45 \pm 0.27$	$1.03 \pm 0.31$
$-\chi^2/dof$	2.17	4.31

Table 4: Constraints from the physical parameters.

move to safeguard against poor mixing and premature convergence.

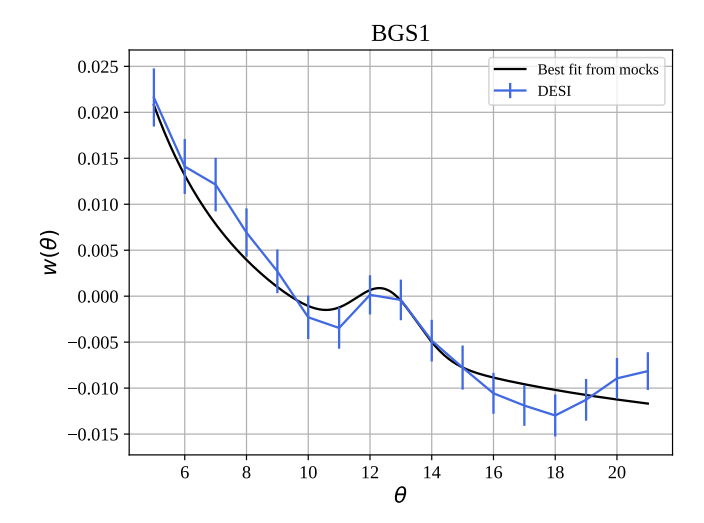
#### 4 Results

First we show the results of the MCMC analysis of the BGS samples in Figs. 3a and 3b. The 68% contour level is a defined ellipsoidal shape for all parameters in both samples, indicating the success of the parameter inference. We summarise the physical results in Table 4, all three results show C>0, indicating the presence of the BAO peak. Both the  $\chi^2/{\rm degrees}$  of freedom ratio are bigger than one but < 5.0, which indicates a robust result.

The best-fit correlation functions are depicted in Fig. 4. The black line represents the best-fit result, while the blue line denotes the empirical measurement with error bars. It is evident that BGS1 and BGS2 align well with the results.

#### 4.1 Cosmological inference

The angular BAO size,  $\theta_{\text{BAO}} = \frac{r_s}{(1+z)D_A(z)}$ , is equal to the known physical size of the sound wave from the early



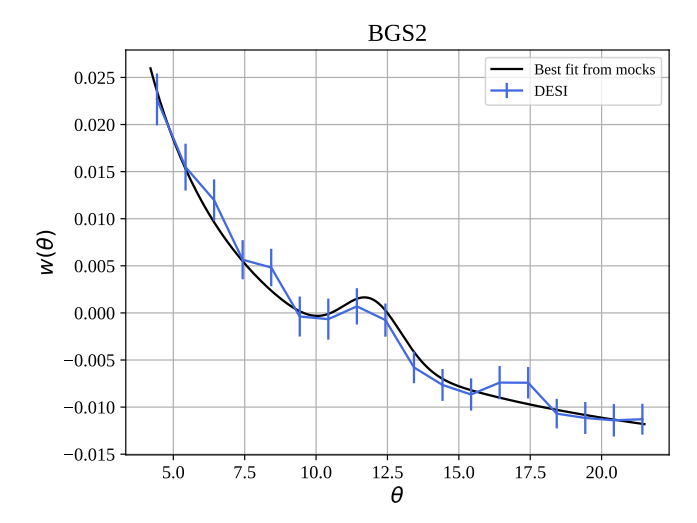


Fig. 4: Two-point correlation function estimated from the data (blue) and best-fit model (black) using the model-free polynomial fit Sánchez et al. [2011].

universe  $(r_s)$  divided by the angular diameter distance to that feature  $(D_A(z))$ , with an extra factor of (1+z) to account for the expansion of the universe since the light was emitted. For us, z is the effective redshift of the sample, the expected  $\theta_{\rm BAO}$  for BGS1 and BGS2 are 9.61 degrees and 8.17 degrees, respectively considering the  $\Lambda$ CDM model with Planck 18 parameters. For a measured feature, we must correct the BAO bump we found from any projection effect, i.e. correct the  $\theta_{fit}$ , here we use a model-dependent version and a statistical version, model-independent, for such correction.

For the model dependent version, we apply the correction from Carvalho et al. [2016] using pyccl [Chisari et al., 2019]. This involves a shift between  $\theta_E(z, \delta z)$ , the expected  $\theta_{\rm BAO}$  given the considered model, for a tracer at wider bin separation  $\delta z$  and the ideal thin-bin case,  $\theta_E(z, \delta z = 0.002)$ . The correction is a normalised difference of the BAO features for the two separations:

$$\theta_{\text{BAO}} = \theta_{fit}(z) + \alpha(z, \delta z)\theta_{fit}(z)$$
 (5)

where  $\alpha$  is

$$\alpha = \frac{\theta_E(z, \delta z = 0.002) - \theta_E(\delta z)}{\theta_E(z, \delta z = 0.002)}$$
(6)

Due to the 3D measurements from DESI favouring the CPL model, we adjusted our fiducial cosmology choice to determine  $\theta_E(z,\delta z=0.002)$  and examined any potential conflict with [Sánchez et al., 2011] and the fiducial correlation function. This concern arises because Sánchez et al. [2011] indicates a larger discrepancy in the polynomial fit with the exact  $\theta_{\rm BAO}$  for  $z_{\rm eff} \leq 0.3$ , relevant to BGS1 and BGS2 who have  $z_{\rm eff} \sim 0.2$ .

The fiducial cosmologies have fixed global parameters based on Planck 18 [Planck Collab., 2020]:  $\Omega_c = 0.2566$ ,  $\Omega_b = 0.0494$ ,  $n_s = 0.9649$ , h = 0.6736,  $\sigma_8 = 0.8111$  and variable parameters  $\Omega_k = (0, 0.001, 0.003, 0.065)$ ,  $w_0 = (-1.0, -0.995, -0.827, -0.7)$ , and  $w_a = (0, -0.75, -1.0)$ 

summarised in Table 5. The choice of parameters was based on the analysis by [DESI collaboration, 2025]. The results can be found in Table 5 where all the combination of parameters can be found, with the first being the Planck 18. These results are in 13 or 14  $\sigma$  tension with Planck 18, all incompatible with  $\Lambda CDM$ . It is clear that the  $\alpha$  correction correction is largely insensitive to the choice of model. However, the error bars are clearly underestimated, as this approach maintains the uncertainties, and possibly biases, of the polynomial fit without including any information regarding the footprint nor the incompleteness of the sample. That could explain the 13 – 14 tension and the small offset between  $\theta_{\rm BAO}$  and  $\theta_{fit}$ .

Although this is the usual approach, Ferreira and Reis [2024] suggested a purely statistical correction to the projection effects, which also contributes to a more robust and complete model agnostic pipeline. The authors wrote  $\alpha$  as a normalised difference between the sample's correlation function and thin bins. The correction parameter is now  $\tilde{\alpha}$ :

$$\tilde{\alpha}_p(\theta) = \frac{\sum_{i=1}^{N_p} w_i(\theta) - w_{\delta z=0}(\theta)}{N_p},$$
(7)

where p denotes the percentile of that difference which in this case we chose the median (p=50) and  $\tilde{\alpha}_p$  is normalised by  $\sqrt{\int |\mathbf{w}_i(\theta) - \mathbf{w}_{\delta z=0}(\theta)|^2} d\theta$ . considering this correction, we rename  $\theta_{\rm BAO}$  as

$$\tilde{\theta}_{BAO}(z_{\text{eff}}) = \theta_{fit} + \tilde{\alpha}(\theta_{fit})\theta_{fit}.$$
 (8)

The result for  $\tilde{\theta}_{BAO}(z_{\text{eff}})$  is shown in Table 6, we see that the error bars are significantly bigger, this is due to the nature of the method, where we include the actual problems of angular counting with this particular sample and its footprint characteristics, being a more realistic estimation of the uncertainties. Here, using  $\tilde{\alpha}$ , BGS1 (BGS2)

	$\theta_{ m BAO} \left[ { m degrees}  ight]$	
Model	BGS1	BGS2
Planck 18 ( $\Omega_k = 0, w_0 = -1, w_a = 0$ )	$12.59 \pm 0.23$	$12.02 \pm 0.27$
$\Lambda$ CDM ( $\Omega_k = 0.001, w_0 = -1, w_a = 0$ )	$12.59 \pm 0.23$	$12.02 \pm 0.27$
$\Lambda \text{CDM } (\Omega_k = 0, w_0 = -1, w_a = 0)$	$12.59 \pm 0.23$	$12.02 \pm 0.27$
$\Lambda$ CDM ( $\Omega_k = 0.065, w_0 = -1, w_a = 0$ )	$12.60 \pm 0.23$	$12.02\pm0.27$
$w$ CDM ( $\Omega_k = 0, w_0 = -0.995, w_a = 0$ )	$12.59 \pm 0.23$	$12.02\pm0.27$
$w$ CDM ( $\Omega_k = 0.001, w_0 = -0.995, w_a = 0$ )	$12.59 \pm 0.23$	$12.02 \pm 0.27$
$w$ CDM ( $\Omega_k = 0, w_0 = -0.995, w_a = 0$ )	$12.59 \pm 0.23$	$12.02 \pm 0.27$
$w$ CDM ( $\Omega_k = 0.065, w_0 = -0.995, w_a = 0)$	$12.60 \pm 0.23$	$12.02\pm0.27$
$w_0 w_a \text{CDM1} \ (\Omega_k = 0, \ w_0 = -0.827, \ w_a = -0.750)$	$12.59\pm0.23$	$12.02\pm0.27$
$w_0 w_a \text{CDM1} \ (\Omega_k = 0.001, \ w_0 = -0.827, \ w_a = -0.750)$	$12.59 \pm 0.23$	$12.02 \pm 0.27$
$w_0 w_a \text{CDM1} \ (\Omega_k = 0, \ w_0 = -0.827, \ w_a = -0.750)$	$12.59 \pm 0.23$	$12.02 \pm 0.27$
$w_0 w_a \text{CDM1} (\Omega_k = 0.065, w_0 = -0.827, w_a = -0.750)$	$12.60 \pm 0.23$	$12.02\pm0.27$
$w_0 w_a \text{CDM2} (\Omega_k = 0, w_0 = -0.700, w_a = -1.000)$	$12.59 \pm 0.23$	$12.02\pm0.27$
$w_0 w_a \text{CDM2} \ (\Omega_k = 0.001, \ w_0 = -0.700, \ w_a = -1.000)$	$12.59 \pm 0.23$	$12.02\pm0.27$
$w_0 w_a \text{CDM2} \ (\Omega_k = 0, \ w_0 = -0.700, \ w_a = -1.000)$	$12.60 \pm 0.23$	$12.02 \pm 0.27$
$w_0 w_a \text{CDM2} (\Omega_k = 0.065, w_0 = -0.700, w_a = -1.000)$	$12.60\pm0.23$	$12.03\pm0.27$

Table 5: Model comparison results for BGS1 and BGS2 using equation 5. That means that the theoretical  $\alpha$  correction does not varies with the model. However, its error bars are not realistic.

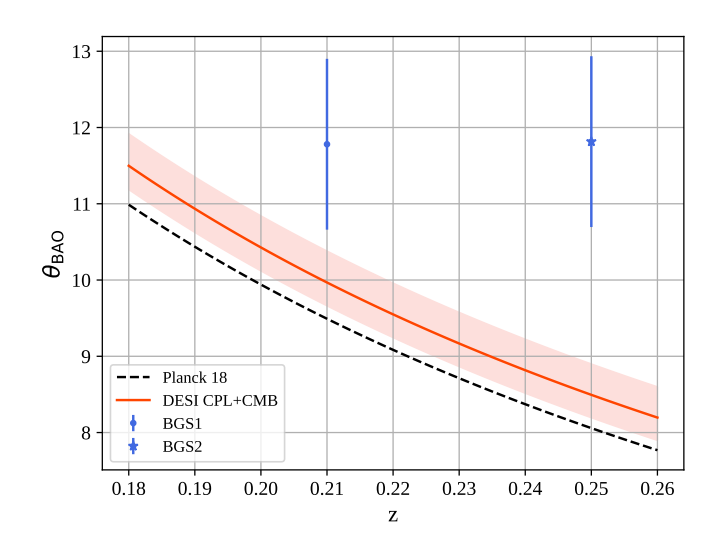


Fig. 5:  $\theta_{\rm BAO}$  with Planck 18 as the dashed-line and the red line is DESI CPL ( $\Omega_m = 0.3069 \pm 0.005, H_0 = 67.97 \pm 0.38, w_0 = -1.79 \pm ^{0.34}_{0.32}, w_a = -1.79 \pm ^{0.48}_{1.0}$ ). The observed points are in blue.

 $\tilde{\theta}_{BAO}$  exhibits a 2.04 $\sigma$  (3.31 $\sigma$ ) deviation from the expected by Planck 18  $\Lambda$ CDM model. Compared to DESI+CMB constrained CPL parameters [DESI collaboration, 2025] ( $\Omega_m = 0.3069 \pm 0.005$ ,  $H_0 = 67.97 \pm 0.38$ ,  $w_0 = -1.79 \pm ^{0.34}_{0.32}$ ,  $w_a = -1.79 \pm 1.0$ ), the tension for BGS1  $\tilde{\theta}_{BAO}$  is at 1.53 $\sigma$  level and BGS2  $\tilde{\theta}_{BAO}$  at 2.62 $\sigma$  level, indicating a moderate preference to CPL, but yet not strong. Our result compared to both models can be visualised in Fig. 5, in red is the DESI CPL and the dashed line in black is Planck 18, our data points are in blue and the red region is the 68% CL of DESI results. This result is robust considering we are

Sample	$ ilde{ heta}_{BAO}(z_{ ext{eff}})$
BGS1	$11.78 \pm 1.12 \deg$
BGS2	$11.81 \pm 1.20 \deg$

Table 6: BAO result using the statistical projection effect correction from equation 8.

including the imperfections of a not yet complete homogeneously observed footprint, not to mention the problems of using a low redshift sample such as BGS. Again, we must state that a more complete sample in future releases may provide strong indicators to which cosmological model is the best, but for now we understand that the DESI DR1 constraints, using  $w(\theta)$  as the BAO probe, are inconclusive.

# 5 Summary

In this work, we studied the angular characteristic of the BAO using DESI BGS samples. We selected the best samples according to their angular density in the sky, this was necessary because DESI DR1 did not have a good sky coverage yet, something that will improve as the survey continues its observation. The consequence of the deep search for the best bin choice is that we ended up with only the BGS sample.

We constructed 1,000 LPT1 mocks and included systematic weights. Since our goal is just to use mocks for the covariance matrix, our number of realisations is sufficient for the analysis. For random mock samples, we used a new approach that, by construction, isotropically distributes the objects over the considered footprint and is numerically very light, as it is based only on integer-number sampling.

The analysis using MCMC was carried out employing broad and uniform priors, thus refraining from giving preference to any particular region for  $\theta_{fit}$ . In this context, the model proposed by Sánchez et al. [2011] was used to fit the calculated correlation function, resulting in  $2 < \chi^2/\text{dof} < 4$ , which demonstrates a robust model fit. The derived outcomes for  $\theta_{fit}$  are 12.54 degrees for BGS1 and 11.97 degrees for BGS2, respectively, all incompatible in many sigma with Planck 18.

Following the application of the projection effect correction using certain cosmological models tested within DESI, our analysis of DR1 reveals minimal differences in  $\theta_{\rm BAO}$ when comparing  $\Lambda$ CDM and CPL models. However, this method is dependent on cosmological parameters and does not consider the footprint imperfections. Thus, we tested Ferreira and Reis [2024]  $\theta_{\rm BAO}$  estimation from a purely statistical comparison with thin bins inside the sample. This more robust approach showed a less dramatic tension with the expected  $\theta_{\rm BAO}$  from Planck 18  $\Lambda{\rm CDM}$  parameters, with BGS1 11.78  $\pm$  1.12 degrees and BGS2 11.81  $\pm$  1.20 degrees but now with apparent preference to the CPL parametrisation: BGS1 is at  $1.53\sigma$  tension level and BGS2 at  $2.62\sigma$  level, which we choose as our main result. This is stable even when accounting for the imperfections of an incomplete footprint and the issues related to employing a low redshift sample like BGS. It is worth noting that future releases with more comprehensive samples might better support alternative cosmological models. Currently, however, we acknowledge that the DESI DR1, with  $w(\theta)$ serving as the BAO probe, does not provide conclusive results.

### Acknowledgements

Paula Ferreira thanks Brazilian funding agency FINEP for the contract under the MultiGPU project 1891/22. Pedro da Silveira Ferreira thanks Brazilian funding agency FINEP (contract 01.22.0505.00) for financial support. This work made use, mostly, of the Milliways HPC computer located at the Instituto de Física in the Universidade Federal do Rio de Janeiro, managed and funded by ARCOS (Astrophysics, Relativity and COSmology research group). The authors made use of one of the Sci-Mind servers machines, developed by the CBPF Lab-IA team. UR thanks the Brazilian National Research Council (CNPq) for the financial support. CRB acknowledges the financial support from CNPq (316072/2021-4) and from FAPERJ (grants 201.456/2022 and 210.330/2022) and the FINEP contract 01.22.0505.00 (ref. 1891/22). This research used data obtained with the Dark Energy Spectroscopic Instrument (DESI). DESI construction and operations is managed by the Lawrence Berkeley National Laboratory. This material is based upon work supported by the U.S. Department of Energy, Office of Science, Office of High-Energy Physics, under Contract No. DE-AC02-05CH11231, and by the National Energy Research Scientific Computing Center, a DOE Office of Science User Facility under the same contract. Additional support for DESI was provided by the

U.S. National Science Foundation (NSF), Division of Astronomical Sciences under Contract No. AST-0950945 to the NSF's National Optical-Infrared Astronomy Research Laboratory; the Science and Technology Facilities Council of the United Kingdom; the Gordon and Betty Moore Foundation; the Heising-Simons Foundation; the French Alternative Energies and Atomic Energy Commission (CEA); the National Council of Humanities, Science and Technology of Mexico (CONAHCYT); the Ministry of Science and Innovation of Spain (MICINN), and by the DESI Member Institutions: www.desi.lbl.gov/collaborating-institutions. The DESI collaboration is honored to be permitted to conduct scientific research on I'oligam Du'ag (Kitt Peak), a mountain with particular significance to the Tohono O'odham Nation. Any opinions, findings, and conclusions or recommendations expressed in this material are those of the author(s) and do not necessarily reflect the views of the U.S. National Science Foundation, the U.S. Department of Energy, or any of the listed funding agencies. AB acknowledges a CNPq fellowship.

# References

- S. Alam et al. The clustering of galaxies in the completed sdss-iii baryon oscillation spectroscopic survey: cosmological analysis of the dr12 galaxy sample. *Monthly Notices of the Royal Astronomical Society*, 470(3):2617–2652, Mar. 2017. ISSN 1365-2966. doi:10.1093/mnras/stx721. URL http://dx.doi.org/10.1093/mnras/stx721.
- J. S. Alcaniz, G. C. Carvalho, A. Bernui, J. C. Carvalho, and M. Benetti. Measuring baryon acoustic oscillations with angular two-point correlation function, 2016. URL https://arxiv.org/abs/1611.08458.
- F. Bernardeau, S. Colombi, E. Gaztañaga, and R. Scoccimarro. Large-scale structure of the universe and cosmological perturbation theory. *Physics Reports*, 367 (1):1–248, 2002. ISSN 0370-1573. doi:10.1016/S0370-1573(02)00135-7.
- G. Carvalho, A. Bernui, M. Benetti, J. Carvalho, and J. Alcaniz. Baryon acoustic oscillations from the sdss dr10 galaxies angular correlation function. *Physical Review D*, 93(2):023530, 2016. doi:0.1103/PhysRevD.93.023530.
- G. Carvalho, A. Bernui, M. Benetti, J. Carvalho, E. de Carvalho, and J. Alcaniz. The transverse baryonic acoustic scale from the sdss dr11 galaxies. *Astroparticle Physics*, 119:102432, 2020. doi:10.1016/j.astropartphys.2020.102432.
- K. C. Chan et al. Dark energy survey year 3 results: Measurement of the baryon acoustic oscillations with three-dimensional clustering. *Physical Review D*, 106(12), Dec. 2022. ISSN 2470-0029. doi:10.1103/physrevd.106.123502. URL http://dx.doi.org/10.1103/PhysRevD.106.123502.
- M. Chevallier and D. Polarski. Accelerating universes with scaling dark matter. International Journal of Modern Physics D, 10(02):213–223, Apr. 2001. ISSN 1793-6594. doi:10.1142/s0218271801000822. URL http://dx.doi.org/10.1142/S0218271801000822.

- N. E. Chisari, D. Alonso, E. Krause, C. D. Leonard, P. Bull, J. Neveu, A. Villarreal, S. Singh, T. McClintock, J. Ellison, Z. Du, J. Zuntz, A. Mead, S. Joudaki, C. S. Lorenz, T. Tröster, J. Sanchez, F. Lanusse, M. Ishak, R. Hlozek, J. Blazek, J.-E. Campagne, H. Almoubayyed, T. Eifler, M. Kirby, D. Kirkby, S. Plaszczynski, A. Slosar, M. Vrastil, and E. L. Wagoner. Core cosmology library: Precision cosmological predictions for lsst. *The Astrophysical Journal Supplement Series*, 242(1):2, May 2019. ISSN 1538-4365. doi:10.3847/1538-4365/ab1658. URL http://dx.doi.org/10.3847/1538-4365/ab1658.
- C.-H. Chuang, F.-S. Kitaura, F. Prada, C. Zhao, and G. Yepes. Ezmocks: extending the zel'dovich approximation to generate mock galaxy catalogues with accurate clustering statistics. *Monthly Notices of the Royal Astronomical Society*, 446(3):2621–2628, 2015. doi:10.1093/mnras/stu2301.
- S. Cole, W. J. Percival, J. A. Peacock, P. Norberg, C. M. Baugh, C. S. Frenk, I. Baldry, J. Bland-Hawthorn, T. Bridges, R. Cannon, M. Colless, C. Collins, W. Couch, N. J. G. Cross, G. Dalton, V. R. Eke, R. De Propris, S. P. Driver, G. Efstathiou, R. S. Ellis, K. Glazebrook, C. Jackson, A. Jenkins, O. Lahav, I. Lewis, S. Lumsden, S. Maddox, D. Madgwick, B. A. Peterson, W. Sutherland, and K. Taylor. The 2dF Galaxy Redshift Survey: power-spectrum analysis of the final data set and cosmological implications. mnras, 362(2):505-534, Sept. 2005. doi:10.1111/j.1365-2966.2005.09318.x.
- S. Cole, W. J. Percival, J. A. Peacock, P. Norberg, C. M. Baugh, C. S. Frenk, I. Baldry, J. Bland-Hawthorn, T. Bridges, R. Cannon, M. Colless, C. Collins, W. Couch, N. J. G. Cross, G. Dalton, V. R. Eke, R. De Propris, S. P. Driver, G. Efstathiou, R. S. Ellis, K. Glazebrook, C. Jackson, A. Jenkins, O. Lahav, I. Lewis, S. Lumsden, S. Maddox, D. Madgwick, B. A. Peterson, W. Sutherland, and K. Taylor. The 2df galaxy redshift survey: power-spectrum analysis of the final data set and cosmological implications. *Monthly Notices of the Royal Astronomical Society*, 362(2):505–534, Sept. 2005. ISSN 1365-2966. doi:10.1111/j.1365-2966.2005.09318.x. URL http://dx.doi.org/10.1111/j.1365-2966.2005.09318.x.
- E. De Carvalho, A. Bernui, G. Carvalho, C. Novaes, and H. Xavier. Angular baryon acoustic oscillation measure at z= 2.225 from the sdss quasar survey. *Journal of Cosmology and Astroparticle Physics*, 2018(04):064, 2018. doi:10.1088/1475-7516/2018/04/064.
- E. De Carvalho, A. Bernui, H. Xavier, and C. Novaes. Baryon acoustic oscillations signature in the three-point angular correlation function from the sdss-dr12 quasar survey. *Monthly Notices of the Royal Astronomical Soci*ety, 492(3):4469–4476, 2020. doi:10.1093/mnras/staa119.
- E. De Carvalho, A. Bernui, F. Avila, C. P. Novaes, and J. Nogueira-Cavalcante. Bao angular scale at zeff= 0.11 with the sdss blue galaxies. *Astronomy & Astrophysics*, 649:A20, 2021. doi:10.1051/0004-6361/202039936.
- DESI collaboration. Desi 2024 vi: cosmological constraints from the measurements of baryon acoustic oscillations. *Journal of Cosmology and Astroparticle Physics*, 2025(02):021, feb 2025. doi:10.1088/1475-

- 7516/2025/02/021. URL https://dx.doi.org/10.1088/1475-7516/2025/02/021.
- DESI Collaboration. Desi dr2 results. i. baryon acoustic oscillations from the lyman alpha forest. *Physical Review D*, June 2025a. ISSN 2470-0029. doi:10.1103/2wwn-xjm5. URL http://dx.doi.org/10.1103/2wwn-xjm5.
- DESI Collaboration. Data release 1 of the dark energy spectroscopic instrument, 2025b. URL https://arxiv.org/abs/2503.14745.
- DESI Collaboration. Desi dr2 results ii: Measurements of baryon acoustic oscillations and cosmological constraints, 2025c. URL https://arxiv.org/abs/2503.14738.
- D. J. Eisenstein et al. Detection of the Baryon Acoustic Peak in the Large-Scale Correlation Function of SDSS Luminous Red Galaxies. *apj*, 633(2):560–574, Nov. 2005. doi:10.1086/466512.
- H. A. Feldman, N. Kaiser, and J. A. Peacock. Power-Spectrum Analysis of Three-dimensional Redshift Surveys. APJ, 426:23, May 1994. doi:10.1086/174036.
- P. S. Ferreira and R. R. R. Reis. Angular correlation function from sample covariance with boss and eboss lrg. *The European Physical Journal C*, 84(5):466, May 2024. ISSN 1434-6052. doi:10.1140/epjc/s10052-024-12808-4.
- D. Foreman-Mackey, D. W. Hogg, D. Lang, and J. Goodman. emcee: The mcmc hammer. *Publications of the Astronomical Society of the Pacific*, 125(925):306–312, Mar. 2013. ISSN 1538-3873. doi:10.1086/670067. URL http://dx.doi.org/10.1086/670067.
- H. Gil-Marín et al. The completed sdss-iv extended baryon oscillation spectroscopic survey: measurement of the bao and growth rate of structure of the luminous red galaxy sample from the anisotropic power spectrum between redshifts 0.6 and 1.0. *Monthly Notices of the Royal Astronomical Society*, 498(2):2492–2531, Aug. 2020. ISSN 1365-2966. doi:10.1093/mnras/staa2455. URL http://dx.doi.org/10.1093/mnras/staa2455.
- J. Hartlap, P. Simon, and P. Schneider. Why your model parameter confidences might be too optimistic. unbiased estimation of the inverse covariance matrix. *Astronomy & Astrophysics*, 464(1):399–404, Dec. 2006. ISSN 1432-0746. doi:10.1051/0004-6361:20066170. URL http://dx.doi.org/10.1051/0004-6361:20066170.
- S. D. Landy and A. S. Szalay. Bias and variance of angular correlation functions. *The Astrophysical Journal*, 412: 64–71, 1993. doi:10.1086/172900.
- M. E. Levi et al. The dark energy spectroscopic instrument (desi), 2019. URL https://arxiv.org/abs/1907. 10688.
- E. V. Linder. Exploring the expansion history of the universe. *Physical Review Letters*, 90(9), Mar. 2003. ISSN 1079-7114. doi:10.1103/physrevlett.90.091301. URL http://dx.doi.org/10.1103/PhysRevLett.90.091301.
- V. Marra and E. G. Chirinos Isidro. A first model-independent radial bao constraint from the final boss sample. Monthly Notices of the Royal Astronomical Society, 487(3):3419–3426, 2019. doi:10.1093/mnras/stz1557.
- R. Menote and V. Marra. Baryon acoustic oscillations in thin redshift shells from boss dr12 and eboss dr16 galax-

- ies. Monthly Notices of the Royal Astronomical Society, 513(2):1600–1608, 2022. doi:10.1093/mnras/stac847.
- B. Nelson, E. B. Ford, and M. J. Payne. Run dmc: An efficient, parallel code for analyzing radial velocity observations using n-body integrations and differential evolution markov chain monte carlo. The Astrophysical Journal Supplement Series, 210(1), 2013. ISSN 1538-4365. doi:10.1088/0067-0049/210/1/11.
- S. Novell-Masot, H. Gil-Marín, L. Verde, J. Aguilar, S. Ahlen, S. Bailey, S. BenZvi, D. Bianchi, D. Brooks, E. Buckley-Geer, et al. Full-shape analysis of the power spectrum and bispectrum of desi dr1 lrg and qso samples. *Journal of Cosmology and Astroparticle Physics*, 2025 (06):005, 2025a. doi:10.1088/1475-7516/2025/06/005.
- S. Novell-Masot et al. Full-shape analysis of the power spectrum and bispectrum of desi dr1 lrg and qso samples. Journal of Cosmology and Astroparticle Physics, 2025(06):005, jun 2025b. doi:10.1088/1475-7516/2025/06/005. URL https://dx.doi.org/10.1088/1475-7516/2025/06/005.
- P. Peebles. Statistical analysis of catalogs of extragalactic objects. i. theory. *Astrophysical Journal, Vol. 185, pp. 413-440 (1973)*, 185:413–440, 1973. doi:10.1086/152431.
- W. J. Percival et al. Baryon acoustic oscillations in the sloan digital sky survey data release 7 galaxy sample. Monthly Notices of the Royal Astronomical Society, 401(4):2148–2168, Feb. 2010. ISSN 1365-2966. doi:10.1111/j.1365-2966.2009.15812.x. URL http://dx.doi.org/10.1111/j.1365-2966.2009.15812.x.
- M. Pinon, A. de Mattia, P. McDonald, E. Burtin, V. Ruhlmann-Kleider, M. White, D. Bianchi, A. Ross, J. Aguilar, S. Ahlen, et al. Mitigation of desi fiber assignment incompleteness effect on two-point clustering with small angular scale truncated estimators. *Journal* of Cosmology and Astroparticle Physics, 2025(01):131, 2025. doi:10.1088/1475-7516/2025/01/131.
- Planck Collab. Planck 2018 results. I. Overview and the cosmological legacy of Planck. Astronomy and Astrophysics, 641:A1, Sept. 2020. doi:10.1051/0004-6361/201833880.
- C. Ramírez-Pérez, J. Sanchez, D. Alonso, and A. Font-Ribera. Colore: fast cosmological realisations over large volumes with multiple tracers. *Journal of Cosmology and Astroparticle Physics*, 2022(05):002, 2022. doi:10.1088/1475-7516/2022/05/002.
- U. Ribeiro et al. A cosmology weakly dependent measurement of 2d baryon acoustic oscillations scale from the southern photometric local universe survey. arXiv preprint 2506.08288, 2025.
- A. Ross et al. The construction of large-scale structure catalogs for the dark energy spectroscopic instrument. Journal of Cosmology and Astroparticle Physics, 2025(01):125, jan 2025. doi:10.1088/1475-7516/2025/01/125. URL https://dx.doi.org/10.1088/1475-7516/2025/01/125.
- S. Salazar-Albornoz, A. G. Sánchez, N. D. Padilla, and C. M. Baugh. Clustering tomography: measuring cosmological distances through angular clustering in thin redshift shells. *Monthly Notices of the Royal Astronomical Society*, 443(4):3612–3623, 08 2014.

- doi:10.1093/mnras/stu1428.
- E. Sánchez, A. Carnero, J. García-Bellido, E. Gaztanaga, F. De Simoni, M. Crocce, A. Cabré, P. Fosalba, and D. Alonso. Tracing the sound horizon scale with photometric redshift surveys. *Monthly Notices of* the Royal Astronomical Society, 411(1):277–288, 2011. doi:10.1111/j.1365-2966.2010.17679.x.
- C. J. Ter Braak and J. A. Vrugt. Differential evolution markov chain with snooker updater and fewer chains. *Statistics and Computing*, 18(4):435–446, 2008. doi:10.1007/s11222-008-9104-9.